Photoionization of atomic sodium near threshold

T. W. Gorczyca[*]
Department of Physics, Western Michigan University, Kalamazoo, Michigan 49008, USA

C. P. Ballance[†]
School of Mathematics and Physics, Queen's University Belfast, Belfast BT7 1NN, Northern Ireland, United Kingdom

M. F. Hasoğlu
Aeronautics and Aerospace Engineering, Hasan Kalyoncu University, 27100 Gaziantep, Turkey

N. R. Badnell
Department of Physics, University of Strathclyde, Glasgow G4 0NG, Scotland, United Kingdom

S. T. Manson[‡]
Department of Physics and Astronomy, Georgia State University, Atlanta, Georgia 30303, USA

D. W. Savin
Columbia Astrophysics Laboratory, Columbia University, New York, New York 10027, USA

(Received 6 September 2023; revised 21 March 2024; accepted 4 April 2024; published 3 May 2024)

R-matrix with pseudostates (RMPS) calculations have been carried out for photoionization of atomic sodium near threshold. The large RMPS atomic orbital and configuration basis allows for very accurate computations of low-energy photoionization cross sections up to ≈30 eV, the energy range for which the RMPS calculations were optimized. Consistency checks for accuracy include, first, the excellent agreement found between length- and velocity-gauge theoretical results, a necessary but not sufficient requirement for having a converged wave function. A second accuracy quantification is the excellent prediction of the position of the Cooper minimum compared to experimental results. Particular attention is paid to the Cooper minimum occurring just above threshold, and the spin-orbit splitting of minima, resulting in a nonzero total cross section. Our RMPS results away from the minimum are found to be lower than the experimental data, and we make the case that the experimental magnitudes are an overestimate. A third important affirmation of the present accuracy is the continuity found between the $3s \rightarrow np$ bound-bound discrete oscillator strength density below threshold—see Wiese *et al.* [W. L. Wiese, M. W. Smith, and B. M. Miles, *Atomic Transition Probabilities, Vol. 2: Sodium Through Calcium; A Critical Data Compilation* (US Government Printing Office, Washington, DC, 1969)]—and the $3s \rightarrow \epsilon p$ bound-continuum RMPS oscillator strength density above threshold. These three somewhat independent tests of the accuracy of the computed cross sections add confidence to our recommending the present RMPS results as the most reliable extant data for low-energy Na photoionization (and the earlier Wiese *et al.* results for the discrete states).

DOI: 10.1103/PhysRevA.109.053102

I. INTRODUCTION

Near-threshold photoionization of atomic Na has long been of interest for basic physics. Theoretical studies have been carried out for photoionization of Na for more than 70 years, beginning with the pioneering Hartree-Fock calculations of Seaton [1], where it was revealed that a minimum in the radial dipole matrix element occurred due to the differing nodal structure of the absorbing electron and the photoelectron, as elucidated even earlier by Bates [2], and now referred to as a Cooper minimum [3]. This makes accurate computation of the near-threshold region problematic, since the details of the very small photoionization cross section in the region of the minimum are highly sensitive to the exact orbitals used (or more precisely, for multichannel calculations as carried out here, the initial and final many-body wave functions). Since that time, the problem of the near-threshold photoionization cross section of Na, in the region of the Cooper minimum, has been considered theoretically in a number of papers (see, e.g., Boyd [4], Smith and LaBahn [5], Weisheit [6], Sukumar and Kulander [7], Aymar [8], Kupilauskiene [9], Petrov *et al.* [10], and Singor *et al.* [11,12]). However, none of these calculations take correlation into account on an *ab initio* basis. There has also been a nonrelativistic close-coupling calculation which used a semiempirical form of the dipole operator [13] along

[*]thomas.gorczyca@wmich.edu
[†]C.Ballance@qub.ac.uk
[‡]smanson@gsu.edu

with a small set of pseudostates that were calculated using an empirical polarization potential. In addition, there have been calculations for other alkali-metal atoms, using sophisticated *ab initio* methods, such as the Dirac-based B-spline R-matrix calculations of Ref. [14] for K $4s$ photoionization in the threshold region, and demonstrated good agreement with experiment. Experimentally, the early work of Hudson and Carter [15] delineated the Cooper minimum in great detail, although the cross section at energies just above the minimum exhibits a behavior that cannot be attributed to the energy structure of the atom and appears to be unphysical. Here we theoretically quantify this Cooper minimum in detail and obtain reliable cross sections in the photon energy range just above threshold. We also quantify the quality of a number of the earlier calculations.

At this point, it is worthwhile to mention why the minimum is known as a Cooper minimum. That zeros (or near zeros) in radial dipole matrix elements caused alkali-metal s-subshell cross-section minima was pointed out by Bates [2], as mentioned above. The phenomenon had been observed by Ditchburn *et al.* [16] confirming earlier observations [17,18]. It was pointed out by Seaton [1] that, because of relativistic (spin-orbit) effects, the zeros in the two continuum ϵp channels in the alkali metals occur at different energies and as a result the minimum in the total cross section does not actually reach zero. Cooper [3] subsequently analyzed the minima and showed that they were a ubiquitous general phenomenon in valence photoionization of atoms throughout the periodic table and not restricted to alkali-metal spectra; for this reason, the minima are designated as Cooper minima.

The rest of the paper is organized as follows. The theoretical methodology of two independent R-matrix approaches is presented in Sec. II. Section III presents our theoretical results and other existing data. Here, the Cooper minimum is studied in detail, including relativistic fine-structure effects, and the continuity of the oscillator strength density from above to below threshold is examined. Concluding remarks as to the findings and the accuracy of these cross sections are given in Sec. IV.

II. THEORETICAL METHODOLOGY

The essential direct process in the low-energy region of interest consists of outer-shell $3s$ photoionization, occurring at the first $2p^6(^1S_0)$ ionization threshold of 5.14 eV, and inner-shell $2p$ photoionization, occurring far higher in energy at about 38 eV for the four various $2p^5 3s(^3P_{2,1,0})$ and $2p^5 3s(^1P_1)$ levels [the two $2s2p^6 3s(^{3,1}S)$ ionization thresholds occur at even higher energies of about 70 eV and exhibit much weaker cross sections]:

$$h\nu + 1s^2 2s^2 2p^6 3s \rightarrow 1s^2 2s^2 2p^6\, \epsilon p \quad (1)$$

$$\rightarrow 1s^2 2s^2 2p^5 3s\, \epsilon s \quad (2)$$

$$\rightarrow 1s^2 2s^2 2p^5 3s\, \epsilon d. \quad (3)$$

Here ϵl denotes the continuum electron orbital of photoelectron energy ϵ and angular momentum l. Also important in the low-energy region between the first ionization threshold of the $Na^+(2p^6)$ ground state and the first excited $Na^{+*}(2p^5 3s[^3P,^1P])$ thresholds is the strong Rydberg series of autoionizing resonances. These are characterized by their principal quantum number n and angular momentum l and enhance the photoionization cross section via

$$\begin{array}{ccc} h\nu + 1s^2 2s^2 2p^6 3s & \longrightarrow & 1s^2 2s^2 2p^5\, 3s\, nl\ (l = 0, 2) \\ & \searrow \quad \downarrow & \\ & & 1s^2 2s^2 2p^6\, \epsilon p. \end{array} \quad (4)$$

As has been studied for almost a century [1–3,13,19], a zero in the cross section occurs near threshold. As mentioned earlier, this is due to a zero in the dipole radial transition $3s \rightarrow \epsilon p$:

$$\sigma \propto \left| \int_0^\infty P_{3s}(r)\, r\, P_{\epsilon p}(r)\, dr \right|^2 \longrightarrow 0. \quad (5)$$

As the continuum energy ϵ is increased from zero above threshold, the final continuum orbital ϵp acquires more nodes in the vicinity of the initial $3s$ orbital and complete cancellation can occur. The length form of the dipole operator is used above, but the general argument remains valid for velocity or acceleration forms of the operator.

Interestingly, the same sensitivity of the cancellation behavior in the near-threshold cross section was also found in the dielectronic recombination of Mg^{2+} [20], which is essentially the time reversal of the photoionization process studied here. That is, the dielectronic recombination of electrons incident on Ne-like Mg^{2+} leading to Na-like Mg^+ plus an emitted photon, $e^- + Mg^{2+} \rightarrow Mg^+ + h\nu$, is isoelectronically the reverse of a photon incident on neutral Na leading to Ne-like Na^+ and an ionized electron, $h\nu + Na \rightarrow Na^+ + e^-$. This indicates that Cooper-minimum-like cancellation features, both for above threshold (bound-continuum) photoionization and for the reverse (free-bound) photorecombination, are ubiquitous features of atomic collisions in general.

The present R-matrix calculations proceeded along two slightly different routes. For the first series of calculations, a more standard R-matrix (RMAT) approach was employed [21–24] using the atomic structure input orbitals and configurations as was first constructed in an earlier study on Na inner-shell photoionization [19]. In that work, the atomic structure was computed using the configuration-interaction code CIV3 [25]. Physical, or spectroscopic, orbitals $nl = \{1s, 2s, 2p, 3s, 3p, 3d, 4s, 4p\}$ were first generated by optimizing on the various $1s^2 2s^2 2p^5 nl$ states of the target Na^+ ion, and additional correlation orbitals, or pseudo-orbitals, $\overline{nl} = \{\overline{5s}, \overline{5p}, \overline{5d}\}$, were included to account for further term dependence and relaxation of orbitals between different target states. This led to an R-matrix atomic "box" size of $R_A = 29.2$ a.u. A large configuration basis was then constructed from the 14 orbitals, which include single and double promotions out of the $1s^2 2s^2 2p^6$ and $1s^2 2s^2 2p^5 3l$ base configurations, allowing for only single occupancy of the $n = 4$ and 5 orbitals. This standard approach is used routinely in photoionization studies and is fairly accurate for systems consisting of only one or two active electrons. The difficulty of this approach has to do with the sensitivity of replicating the small cross section in the Cooper minimum region just above threshold, as we shall see.

For a more complete representation, a second, larger calculation was performed using the R-matrix with pseudostates (RMPS) method [21]. The particular code used is that first

described by Gorczyca and Badnell [26]. Physical orbitals for the ground-state configuration of Na^+ ($\{1s, 2s, 2p, 3s, 3p\}$), and additional physical orbitals ($\{3d, 4s, 4p, 4d, 4f\}$) were first generated and then an additional, large set of Laguerre pseudo-orbitals $\{\overline{5}s, \overline{5}p, \overline{5}d, \overline{5}f\}, \ldots, \{\overline{12}s, \overline{12}p, \overline{12}d\}$, with nonphysical, more compact nodal structure, were constructed. The resulting R-matrix box size used here is $R_A = 37.2$ a.u. All 79 configurations for the Ne-like Na^+ target states that include single-electron promotions from the $1s^2 2s^2 2p^6$ Na^+ ground-state configuration are included, thereby spanning the $3s$ photoionization target continuum with a fairly large and dense basis. In other words, the calculation includes an excellent approximation to the portion of a complete set that spans the space insofar as the $3s$ photoionization calculation near threshold is concerned. On the other hand, no electron promotions are included out of the excited $1s^2 2s^2 2p^5 3s$ target, therefore the atomic structure of the excited state is not as complete, and the $2p$ photoionization cross section is not expected to be as reliable.

The pseudo-orbitals $5 \leqslant \overline{n} \leqslant 12$ are chosen to be of Laguerre orbital form [27]:

$$u_{nl}(r) = N_{nl}(\lambda_{nl} Z r)^{l+1} e^{-\lambda_{nl} Z r/2} L_{n+l}^{2l+1}(\lambda_{nl} Z r). \qquad (6)$$

Here L_{n+l}^{2l+1} is an associated Laguerre polynomial [28], N_{nl} is a normalization constant, $Z = 1$ is the effective charge seen by the outer-most electron from the Na^+ residual ion, and the variable λ_{nl} allows for variation of the spatial extent of orbitals. We chose the default value $\lambda_{nl} = 1$ for generating a compact basis representation, and $\overline{n}_{\max} = 12$ for the highest principal quantum number for the pseudo-orbital basis. This results in an inner-region radius of $R_A = 37.2$ a.u. for 99.99% of the pseudo-orbital probability. Further discussion of the convergence of cross sections with regard to the choice of a pseudostate basis is discussed in the results section and has also been addressed, using our same RMPS codes, in recent works on double L-shell photoionization of oxygen [29] and double K-shell photoionization of neon [30].

III. RESULTS AND DISCUSSION

A. Nonrelativistic 3*s* and 2*p* photoionization

Photoionization cross sections for atomic Na near the $3s$ threshold were calculated in LS coupling using both the RMAT and the RMPS methodologies, as described above, in both length and velocity gauges. The results are shown in the top panel of Fig. 1 along with the only experimental results that we are aware of, namely those of Hudson and Carter [15]. Over the range from threshold to the first inner-shell resonance at about 30 eV, the theoretical curves are qualitatively similar. However, the RMAT results show significant differences between length and velocity gauges, while the RMPS length and velocity cross sections are seen to be virtually identical. Since equality of length and velocity cross section is a necessary condition for accuracy of a photoionization calculation, this equality strongly suggests that the RMPS cross section is the more accurate. This result also shows that the addition of the pseudostates results in a significantly larger basis set that does a better job of spanning the space.

Note also that the RMAT cross section at threshold is more than a factor of 5 larger than the RMPS result. This is

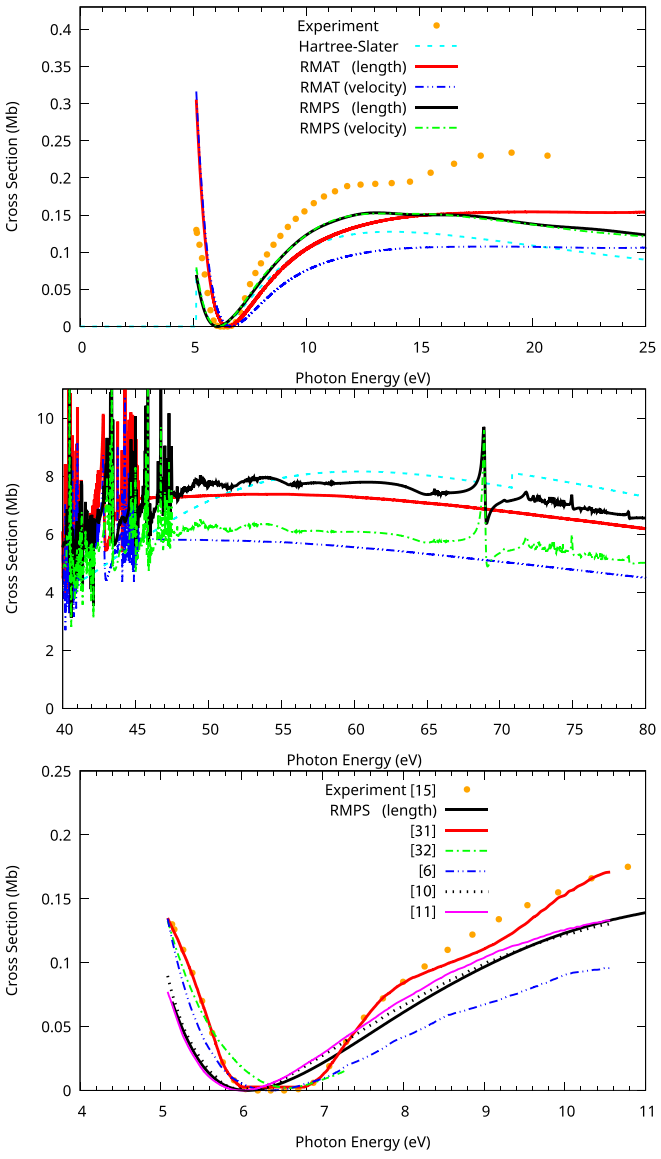

FIG. 1. Neutral Na photoionization cross section: RMAT and RMPS results in length and velocity gauges, Hartree-Slater fitted calculations [31], and experimental [15] results. The cross section is given in units of Mb (10^{-18} cm^2). Also shown are results from Singor *et al.* [11,12], and additional data from Hudson [32], Marr and Creek [33], Petrov *et al.* [10], and Weisheit [6] as extracted from Fig. 6 of Singor *et al.* [11].

because the RMAT Cooper minimum is at a higher energy. Furthermore, the RMAT length and velocity cross sections are in excellent agreement below the Cooper minimum (but not above). This shows that while length-velocity agreement is a *necessary* condition for accuracy, it is not *sufficient*. The length-velocity agreement for the RMAT cross section occurs only for a very small energy range below the Cooper minimum, while the agreement for RMPS length and velocity cross sections from threshold holds up to the region of the $2p$ ionization threshold, above which the present theoretical treatment is not tailored.

Excellent agreement between our RMPS results and experiment is found in the region of the Cooper minimum as

to both the location of the minimum and the shape of the cross section. However, the experimental cross section is a little higher and exhibits a completely unphysical inflection point at about 15 eV. Given the length-velocity equality of the RMPS cross sections, we suggest that the experiment, which was performed more than a half century ago, suffers from systematic errors, making the cross section a little too high and producing the unphysical inflection point. This agrees with the conclusions of Butler and Mendoza [13] concerning the experiment. In short, we believe that the theoretical RMPS cross section is the most accurate extant representation of atomic Na in the energy region from threshold to 30 eV. (At higher energies, where the $2p$ photoionization channels open, the length and velocity theoretical results differ, indicating uncertainty in the cross sections, which, as discussed earlier, is because the single promotions out of the excited core $1s^22s^22p^53s \rightarrow 1s^22s^22p^43s\overline{nl}$ were not included).

Also shown in the top panel of Fig. 1 is the Hartree-Slater central-field-approximation cross section. This agrees fairly well with the RMPS result, despite the simplicity of the Hartree-Slater calculation. This is partially due to the simplicity of the situation, a single electron outside closed shells, and due to the fact that the compendium of "Hartree-Slater" data, as encapsulated in the FORTRAN module from Verner and Yakovlev [31], has been moved to the experimental threshold. Note also that, within this simple approximation, length and velocity gauges agree since Hartree-Slater ionization energies are used for both, so only a single cross section is shown.

Although not the main focus of this paper, at higher energies, where the $2p$ photoionization channels open, the situation is rather different (see the middle panel of Fig. 1). Both RMAT and RMPS results show significant quantitative differences between length- and velocity-gauge results. This occurs because the calculations were optimized for the low-energy $3s$ ionization region and shows that the pseudostates need to be tailored to the specific energy region of interest. This is further underscored by the fact that, in this energy range, the length forms of the RMAT cross sections, without pseudostates, and the RMPS cross sections, with pseudostates, are in quite good agreement, as is the case for the RMAT and RMPS velocity gauge results, thereby demonstrating that the pseudostates that were optimized for the low energy are not particularly helpful at these higher energies.

We also note that the small oscillations in the RMPS cross sections in this energy range are due to the discrete nature of the pseudo-orbitals approximating a second continuum, and should be averaged over energy. However, the large oscillation in the RMPS cross sections in the 70-eV region is the $2s \rightarrow 3p$ resonance. The standard RMAT calculations, on the other hand, include no $2p \rightarrow \overline{np}$ pseudostates, and thus there are no pseudoresonance oscillations. Since the pseudostates were optimized for $3s$ photoionization, these resonant cross sections, like the continuum cross sections above the $2p$ thresholds, are not entirely accurate (the length and velocity results for below-threshold oscillator strength and above-threshold oscillator strength density both show a $\approx$20% discrepancy.)

A separate study was also conducted in order to assess the convergence of the pseudo-orbital wave-function description and the computed results. To within 3%, the photoionization cross section below the lowest $2p$ threshold that we obtain, using both an $n = 14$, $l = 3$ pseudo-orbital basis and $n = 14$, $l = 4$, is the same as that reported here ($n = 12$, $l = 3$), thus demonstrating convergence in both n and l.

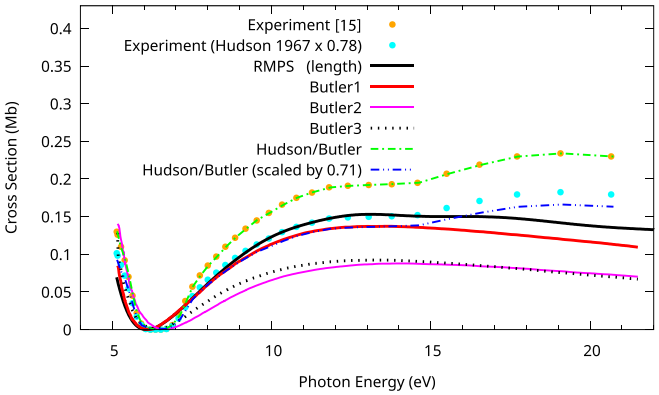

FIG. 2. RMPS vs experimental, scaled experimental, and various models from the close-coupling calculations of Butler and Mendoza [13] using an effective dipole operator and an empirical, three-parameter model polarization potential to obtain pseudostates.

A comparison of the present RMPS cross section with various semiempirical calculations is shown in the bottom panel of Fig. 1. Significant differences are seen between the present results and those of Refs. [6,32,33]. However, reasonable agreement is found with the results of Petrov *et al.* [10] and Singor *et al.* [11]. Evidently, the essential physics of the problem is included in their semiempirical potentials. The present improvement using the larger RMPS basis set, as opposed to the smaller RMAT basis, demonstrates that a large basis expansion is necessary for a good representation of the wave function, and the lower-order expansions used in the earlier work of Petrov *et al.* [10] and Singor *et al.* [11] are not expected to yield an adequate wave-function description without an empirical, adjustable model potential addition.

A comparison of the present results with various levels of the close-coupling calculation of Butler and Mendoza [13] is shown in Fig. 2 along with experiment and scaled experiment. The agreement of the present result with the best calculation of Butler and Mendoza [13] is quite good overall, although there is about a 20% difference above about 20 eV. Note, however, that while our present calculation shows excellent agreement between length and velocity gauges over this entire energy range, the results of Butler and Mendoza [13] present only length gauge so how length and velocity cross sections compare is unknown. It was suggested by Butler and Mendoza [13] that the experimental results should be scaled by a factor of 0.71, shown in Fig. 2, but our present results indicate that it should be scaled by a factor of 0.78, also shown in the figure. This scaling is seen to lead to excellent agreement below the unphysical hump in the experimental data.

B. Fine-structure effects in 3*s* photoionization

To assess the possibility of relativistic effects, the RMPS calculation has also been performed at the Breit-Pauli (BP) level, in addition to the *LS* calculations presented in the previous figures. The comparison of the RMPS cross

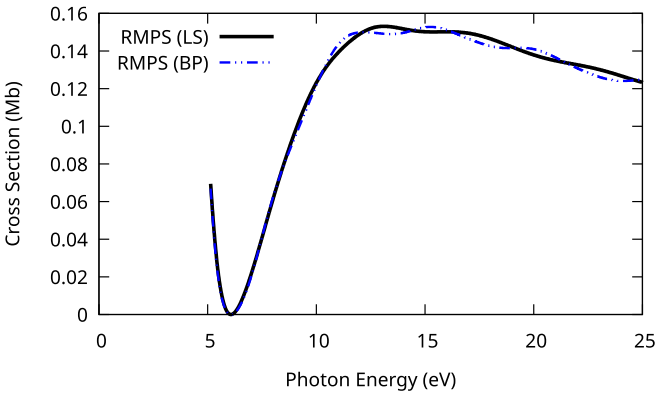

FIG. 3. RMPS neutral Na photoionization cross section from both nonrelativistic (*LS*-coupled) and semirelativistic Breit-Pauli (BP, jK-coupled) calculations, using the length gauge (the velocity gauge results are nearly identical in this energy range).

sections computed in the two different approximations, BP vs *LS*, is shown in Fig. 3, where it is evident that they are virtually identical. Furthermore, the BP length and velocity gauge cross sections are almost identical, as was found for the *LS* cross section at these energies. At the higher energies, above about 10 eV, both curves show small modulations, with the BP results being more so; these are unphysical and arise from the discretization of the continuum, and in going from the simpler *LS* calculations to the more complex BP calculations, it was necessary to reduce the number of continuum basis orbitals per channel from 35 to 18. In any case, the *LS* and BP RMPS cross sections are in excellent agreement in the threshold region and in the vicinity of the Cooper minimum.

It is of interest to look in detail at what happens at the minimum. The cross section does not go to zero for several reasons, the most important of which is that, from a relativistic point of view, there are actually two minima, $3s \rightarrow \epsilon p_{1/2}$ and $3s \rightarrow \epsilon p_{3/2}$, separated very slightly in energy; this idea was first reported more than 70 years ago [1]. The situation is shown in Fig. 4 where it is evident that the cross-section minimum, the sum of the two individual relativistic cross sections, is very much different from the cross sections at the minima of the individual channels. Specifically,

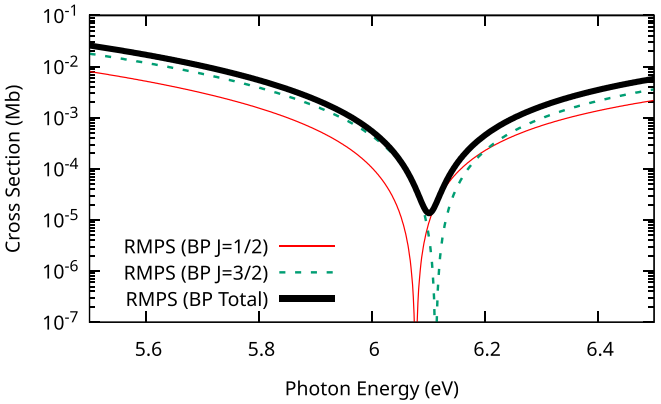

FIG. 4. Neutral Na photoionization cross sections for each of the two independent $J = 1/2$ and $3/2$ fine-structure components.

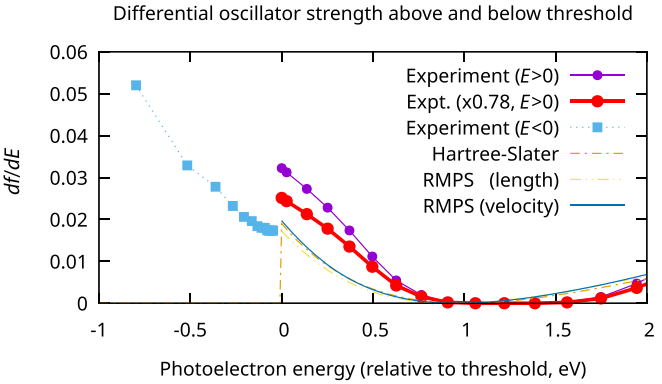

FIG. 5. Energy-differential oscillator strength density for the $3s \rightarrow \epsilon p$ direct photoionization above threshold ($E > 0$) [15] and the $3s \rightarrow np$ discrete states below threshold ($E < 0$) [35]. Also shown above threshold are the Hartree-Slater results of Verner and Yakovlev [31] and the present RMPS length and velocity results in the vicinity of the Cooper minimum.

the total $3s$ cross section reaches a minimum value of about 1.36×10^{-5} Mb, while the individual relativistic $1/2$ and $3/2$ cross sections minimize at 1.02×10^{-9} and 3.60×10^{-9} Mb, respectively. It is thus clear that the relativistic splitting of the Cooper minimum dramatically changes the cross section.

The other reason that the cross sections do not go to zero at the Cooper minimum is the existence of interchannel coupling [34], which is essentially configuration interaction in the continuum and causes the dipole matrix elements to be complex. While both the real and imaginary parts of the matrix element might go to zero in the Cooper minimum region, the two do not go to zero at exactly the same energy, so the magnitude of the matrix element is never zero. This also applies to the nonrelativistic *LS*-coupling matrix element, which is also found to display a nonzero minimum that nevertheless is many orders of magnitude smaller than the BP RMPS $3s$ cross section at the Cooper minimum. However, even though the *LS* and individual relativistic cross sections do not go to zero, their minimum values are extremely small, indicating that, in these cases, the effects of interchannel coupling are also quite small.

C. Oscillator strength density continuity across threshold

Note that the oscillator strength distribution for a given channel must be continuous across the ionization threshold. In other words, the discrete optical oscillator strengths, transformed into oscillator strength per unit energy, must match continuously into the continuum differential oscillator strength, which is simply a constant multiplied by the photoionization cross section. As a consistency check on the threshold cross section, the experimental [35] differential oscillator strength over the discrete range below the ionization threshold is shown in Fig. 5, along with the present RMPS and experimental cross sections converted to differential oscillator strength. The above and below oscillator strength densities are computed as

$$\frac{df}{dE} = \begin{cases} f_n^{\text{absorb}}(n-\mu_n)^3, & E < 0 \\ \sigma/\beta, & E > 0 \end{cases} \tag{7}$$

where $\beta = (\pi k_e e^2 h/m_e c) = 109.7626$ Mb eV where k_e is Coulomb's constant, e is the charge of the electron, h is Planck's constant, m_e is the electron mass, c is the speed of light, and μ_n is the quantum defect, which approaches the high-n asymptotic value $\mu = 0.839$ [36] for the strong ns absorption series. An alternate, convenient way to evaluate the conversion factor is by using the equivalent form $\beta = (2\pi a_0)^2 \alpha\, I_{\rm H}$, where a_0 is the Bohr radius, α is the fine-structure constant, and $I_{\rm H}$ is the ionization energy of hydrogen, explicitly in units of area times energy. The density below threshold is simply the discrete oscillator strength per Rydberg element [35] divided by the energy width of each resonance:

$$\begin{aligned} df/dE &= f_n^{\rm absorb}/(E_{n+1/2} - E_{n-1/2}) \\ &= \frac{f_n^{\rm absorb}}{E_{\rm a.u.}/2(n+1/2-\mu_n)^2 - E_{\rm a.u.}/2(n-1/2-\mu_n)^2} \\ &= f_n^{\rm absorb}(n-\mu_n)^3, \end{aligned} \tag{8}$$

where $E_{\rm a.u.} = 27.2$ eV is an atomic unit of energy. The density above threshold can be computed from the cross section via the relationship $\sigma = \beta\,(\frac{df}{dE})$ [37].

As can be seen, the experimental discrete region oscillator strength distribution matches quite well to the theoretical RMPS threshold value, thereby demonstrating that the RMPS cross section is quite consistent with the extrapolation of the discrete oscillator strengths. The experimental threshold photoionization cross section is significantly higher and needs to be divided by a factor of about 1.3 to agree with the discrete extrapolation. This gives further weight to our contention that the present RMPS Na photoionization cross sections are the most accurate representation of the $3s$ photoionization cross section in the energy range from threshold to 30 eV (above which the $2p$ photoionization, which is not converged here, becomes important), and that the experimental cross section is too large by an approximately constant factor of $\approx$1.3.

IV. CONCLUSION

The near-threshold photoionization of Na, which has been of interest to the atomic theory community for 70 years, has been reexamined using state-of-the-art R-matrix theoretical techniques. Revisited standard R-matrix calculations [19] produced results that showed disagreement between length and velocity results in the low-energy region. This is to be contrasted with our new R-matrix with pseudostates calculations, which included a larger virtual $3s$ excitation basis and produced length and velocity results in good agreement with each other. The RMPS calculations predict a Cooper minimum location and shape that are in quite good agreement with the only available experimental data [15], which is to be contrasted with the RMAT results that predict too high of an energy for the Cooper minimum. This Cooper minimum region was examined in detail using semirelativistic Breit-Pauli R-matrix analysis to reveal small but non-negligible fine-structure channel splitting and resultant nonzero cross sections at the minimum. Further consistency of the seemingly converged RMPS results has been established by the continuity between the above-threshold photoionization cross sections and the below-threshold experimental discrete absorption oscillator strengths [35]. We consider these RMPS results to be the most reliable low-energy Na photoionization cross sections available. We also note that the existing experimental data [15,38] are larger than theory by a factor of about 1.3 in the oscillator strength density at threshold and also display an unphysical inflection point somewhat above the Cooper minimum. Given that the experiment was performed more than a half century ago, as well as the discrepancies with theory and the discrete oscillator strengths, it would appear that the time is ripe for a laboratory reexamination of the near-threshold Na $3s$ photoionization cross section.

It is also useful to point out that the methodology adopted herein can be applied to the entire Na isoelectronic sequence, and it is likely to be more accurate for the higher-Z members of the sequence. This is because the part of the Hamiltonian that is approximated is the noncentral interelectron interaction that becomes a relatively smaller component of the potential, with increasing Z.

Finally, this paper provides an important reminder about the use of pseudostates. It was seen that their inclusion made a significant difference in the equality of the low-energy $3s$ photoionization cross section in length and velocity gauges, as compared to the calculation without such pseudostates. But at the higher energies, where the $2p$ subshell can be excited or ionized, these same pseudostates were not very helpful. This shows that the pseudostates must be tailored for the particular case and energy region of interest. In other words, to do an accurate calculation in the energy range above the $2p$ excitation threshold, a completely different set of pseudostates, including promotions out of the $2p^5 3s$ excited final Na^{+*} ionic state, must be generated to fit the task.

ACKNOWLEDGMENTS

T.W.G. was supported in part by NASA APRA Grants No. NNX11AF32G and No. 80NSSC20K0498. N.R.B. was supported by STFC UK APAP Network Grant No. ST/V000683/1. The work of S.T.M. was supported by the U.S. Department of Energy, Office of Basic Sciences, Division of Chemical Science, Geosciences and Biosciences under Grant No. DE-FG02-03ER15428. D.W.S. was supported, in part, by NASA Grant No. 80NSSC22K0099. We thank R. M. Killen for pointing out the importance of Na photoionization for planetary science.

[1] M. J. Seaton, Proc. R. Soc. A **208**, 418 (1951).
[2] D. R. Bates, Mon. Not. R. Astron. Soc. **106**, 432 (1946).
[3] J. W. Cooper, Phys. Rev. **128**, 681 (1962).
[4] A. H. Boyd, Planet. Space Sci. **12**, 729 (1964).
[5] R. L. Smith and R. W. LaBahn, Phys. Rev. A **2**, 2317 (1970).
[6] J. C. Weisheit, Phys. Rev. A **5**, 1621 (1972).
[7] C. V. Sukumar and K. C. Kulander, J. Phys. B **11**, 4155 (1978).
[8] M. Aymar, J. Phys. B **11**, 1413 (1978).

[9] A. Kupliauskiene, Phys. Scr. **53**, 149 (1996).
[10] I. D. Petrov, V. L. Sukhorukov, and H. Hotop, J. Phys. B **32**, 973 (1999).
[11] A. Singor, D. Fursa, I. Bray, and R. McEachran, Atoms **9**, 42 (2021).
[12] A. Singor, D. V. Fursa, I. Bray, and R. P. McEachran, At. Data Nucl. Data Tables **143**, 101474 (2022).
[13] K. Butler and C. Mendoza, J. Phys. B **16**, L707 (1983).
[14] O. Zatsarinny and S. S. Tayal, Phys. Rev. A **81**, 043423 (2010).
[15] R. D. Hudson and V. L. Carter, J. Opt. Soc. Am. **57**, 651 (1967).
[16] R. W. Ditchburn, J. Tunstead, and J. G. Yates, Proc. R. Soc. A **181**, 386 (1943).
[17] R. W. Ditchburn, Proc. R. Soc. A **117**, 486 (1928).
[18] E. O. Lawrence and N. E. Edlefsen, Phys. Rev. **34**, 1056 (1929).
[19] D. Cubaynes, H. L. Zhou, N. Berrah, J. M. Bizau, J. D. Bozek, S. Canton, S. Diehl, X. Y. Han, A. Hibbert, E. T. Kennedy, S. T. Manson, L. Voky, and F. J. Wuilleumier, J. Phys. B **40**, F121 (2007).
[20] J. Fu, T. W. Gorczyca, D. Nikolic, N. R. Badnell, D. W. Savin, and M. F. Gu, Phys. Rev. A **77**, 032713 (2008).
[21] P. G. Burke, *R-Matrix Theory of Atomic Collisions* (Springer, New York, 2011).
[22] K. A. Berrington, W. B. Eissner, and P. H. Norrington, Comput. Phys. Commun. **92**, 290 (1995).
[23] N. R. Badnell, http://amdpp.phys.strath.ac.uk/tamoc/ (2022).
[24] C. P. Ballance, connorb.freeshell.org (2022).
[25] A. Hibbert, Comput. Phys. Commun. **9**, 141 (1975).
[26] T. W. Gorczyca and N. R. Badnell, J. Phys. B **30**, 3897 (1997).
[27] N. R. Badnell and T. W. Gorczyca, J. Phys. B **30**, 2011 (1997).
[28] M. Abromowitz and I. A. Stegun, *Handbook of Mathematical Functions* (US Government Printing Office, Washington, DC, 1972).
[29] T. W. Gorczyca, C. P Ballance, S. T. Manson, D. Kilcoyne, and W. C. Stolte, Phys. Scr. **96**, 064005 (2021).
[30] S. H. Southworth, S. Li, D. Koulentianos, G. Doumy, L. Young, D. A. Walko, R. Püttner, D. Céolin, R. Guillemin, I. Ismail, O. Travnikova, M. N. Piancastelli, M. Simon, S. T. Manson, and T. W. Gorczyca, Phys. Rev. A **107**, 023110 (2023).
[31] D. A. Verner and D. G. Yakovlev, Astron. Astrophys. Suppl. Ser. **109**, 125 (1995).
[32] R. D. Hudson, Phys. Rev. **135**, A1212 (1964).
[33] G. V. Marr and D. M. Creek, Proc. R. Soc. A **304**, 233 (1968).
[34] U. Fano, Phys. Rev. **124**, 1866 (1961).
[35] W. L. Wiese, M. W. Smith, and B. M. Miles, *Atomic Transition Probabilities, Vol. 2: Sodium Through Calcium; A Critical Data Compilation* (US Government Printing Office, Washington, DC, 1969).
[36] A. E. Kramida, Y. Ralchenko, J. Reader, and NIST ASD Team, NIST Atomic Spectra Database (Version 5.3) (National Institute of Standards and Technology, Gaithersburg, MD, 2023), http://physics.nist.gov/asd.
[37] H. A. Bethe and E. E. Salpeter, Handbuch Phys. **7**, 88 (1957).
[38] R. D. Hudson and V. L. Carter, J. Opt. Soc. Am. **58**, 227 (1968).